Gunter Heymann* and Elisabeth Selb

$Li_2Pt_3Se_4$: a new lithium platinum selenide with jaguéite-type crystal structure by multianvil high-pressure/high-temperature synthesis

DOI 10.1515/znb-2016-0165
Received July 25, 2016; accepted August 3, 2016

Abstract: The monoclinic lithium platinum selenide $Li_2Pt_3Se_4$ was obtained *via* a multianvil high-pressure/high-temperature route at 8 GPa and 1200°C starting from a stoichiometric mixture of lithium nitride, selenium, and platinum. The structure of the ternary alkali metal-transition metal-selenide was refined from single-crystal X-ray diffractometer data: $P2_1/c$ (no. 14), $a = 525.9(2)$, $b = 1040.6(2)$, $c = 636.5(2)$ pm, $\beta = 111.91(1)°$, $R1 = 0.0269$, $wR2 = 0.0569$ (all data) for $Li_2Pt_3Se_4$. Furthermore, the isostructural mineral phases jaguéite ($Cu_2Pd_3Se_4$) and chrisstanleyite ($Ag_2Pd_3Se_4$) were reinvestigated in their ideal stoichiometric ratio. The syntheses of the mineral phases were also carried out under multianvil conditions. Single-crystal data revealed a hitherto not described structural disorder of the transition metal atoms.

Keywords: chrisstanleyite; crystal structure; high-pressure; jaguéite; transition metal-selenide.

1 Introduction

In 2004, Paar [1] reported the discovery of a new mineral with the simplified formula $Cu_2Pd_3Se_4$ (jaguéite) in a telethermal selenide vein-type deposit at the El Chire prospect. This mineral is a copper analog of $Ag_2Pd_3Se_4$ (chrisstanleyite) [2], and in general, the two minerals occur associated and partially intergrown. Electron microprobe analyses of natural jaguéite ($Cu_{1.9}Ag_{0.1}Pd_3Se_4$), and chrisstanleyite ($Ag_{1.6}Cu_{0.4}Pd_3Se_4$) revealed a substitution of about 5% of copper atoms by silver, and of 20% silver atoms by copper, respectively. Their crystal structures were determined by Topa [3], exhibiting a new monoclinic structure type with palladium in a square planar selenium coordination. Systematic investigations of phase relations with the prospect of new compounds in the system Ag–Pd–Se were performed by Vymazalová [4]. Besides $Ag_2Pd_3Se_4$, three other phases ($AgPd_3Se$ [5], $(Ag,Pd)_{22}Se_6$ [6], and $Ag_6Pd_{74}Se_{20}$ [4]) were reported in the temperature range from 350 to 530°C. In the system Cu–Pd–Se, jaguéite ($Cu_2Pd_3Se_4$) is the hitherto only representative.

In addition to these studies, we have investigated the $A_2M_3X_4$ chalcogenides under high-pressure/high-temperature conditions, and have synthesized isostructural sulfide compounds containing lithium as *A*, Pd/Pt as *M*, and sulfur as *X* atoms for the first time [7]. Because of their variety of crystal structures and physical properties like magnetism, metal-insulator transitions [8], superconductivity [9], or magnetoresistance [10, 11], metal-rich chalcogenides [12–14] have attracted considerable interest in solid state chemistry, physics, and material science during the last decades. Ternary lithium-transition metal-chalcogenides are mainly known for the early *d*-block elements. Generally, they form layered structure types with intercalated lithium atoms, potentially attractive for application as lithium ion-conducting materials [15–17]. In contrast, the jaguéite structure type of the title compound is an open framework structure and solid state ^{7}Li NMR experiments on the compounds $Li_2(Pd,Pt)_3S_4$ showed no mobility of the lithium atoms inside the channels [7].

In this contribution, we focused on the corresponding lithium platinum selenide, $Li_2Pt_3Se_4$. Furthermore, we reinvestigated the isostructural mineral phases jaguéite ($Cu_2Pd_3Se_4$) and chrisstanleyite ($Ag_2Pd_3Se_4$) in their ideal stoichiometric ratio. Here, we present the syntheses and the crystal structures of $Li_2Pt_3Se_4$, $Ag_2Pd_3Se_4$, and $Cu_2Pd_3Se_4$.

2 Experimental

2.1 High-pressure/high-temperature syntheses

Starting materials for the multianvil high-pressure/high-temperature synthesis of $Li_2Pt_3Se_4$, according to Eq. 1,

***Corresponding author: Gunter Heymann,** Institut für Allgemeine, Anorganische und Theoretische Chemie, Leopold-Franzens-Universität Innsbruck, Innrain 80–82, A-6020 Innsbruck, Austria, Fax: +43(0)512-507 57099, E-mail: Gunter.Heymann@uibk.ac.at
Elisabeth Selb: Institut für Allgemeine, Anorganische und Theoretische Chemie, Leopold-Franzens-Universität Innsbruck, Innrain 80–82, A-6020 Innsbruck, Austria

was a stoichiometric mixture of Li_3N (purity > 99.4%, Alfa Aesar), platinum sponge (purity > 99.8%, Strem Chemicals, Inc.), and selenium powder (purity > 99.9%, Fluka). Similarly, for syntheses of the isostructural compounds $A_2Pd_3Se_4$ (A = Ag, Cu), according to Eq. 2, stoichiometric mixtures of silver powder (purity > 99.9%, Strem Chemicals, Inc.) or copper powder (purity > 99%, Sigma Aldrich) in combination with palladium powder (purity > 99.95%, Strem Chemicals, Inc.) and selenium powder (purity > 99.9%, Fluka) were used.

$$2\,Li_3N + 9\,Pt + 12\,Se \xrightarrow{8\,GPa/1200\,^\circ C} 3\,Li_2Pt_3Se_4 + N_2 \quad (1)$$

$$2\,A + 3\,Pd + 4\,Se \xrightarrow{8\,GPa/1200\,^\circ C} A_2Pd_3Se_4\ (A = Ag, Cu) \quad (2)$$

The mixtures of the starting materials were milled and loaded into 18/11-assembly crucibles made of hexagonal boron nitride (HeBoSint® P100, Henze BNP GmbH, Kempten, Germany). Because of the air and moisture sensitivity of lithium nitride required for the synthesis of $Li_2Pt_3Se_4$, it was essential to prepare the assembly under inert gas atmosphere. To compress the walker module of the press up to the desired pressure of 8 GPa, 210 min were necessary. After reaching the synthesis pressure the samples were heated to 1200°C within 15 min, kept constant for 10 min and were gently cooled down for the next 2 h to 500°C, followed by quenching the samples to room temperature. This annealing process under pressure can improve the crystallinity of the samples. After finishing the decompression process of the press, the samples could be easily separated from the surrounding assembly materials and no reaction with the crucible material was observed. Further information about the technique and the construction of the different assemblies can be found in numerous references [18–21]. The polycrystalline samples were stable in air and appeared silvery with metallic lustre. By milling, they turned into dark gray powders.

2.2 X-ray diffraction and data collections

Characterization of the polycrystalline high-pressure samples was performed by powder diffraction on a STOE Stadi P diffractometer with (111)-curved Ge-monochromatized $MoK_{\alpha 1}$ radiation (λ = 70.93 pm) in transmission geometry. The powdered samples were mounted between acetate films and fixed with high-vacuum grease. The diffraction intensities were collected by a Dectris MYTHEN2 1K microstrip detector with 1280 strips.

Based on the parameters derived from the single-crystal structure model, Rietveld refinement of $Li_2Pt_3Se_4$ was done with the DIFFRAC^{plus}-TOPAS® 4.2 software package (Bruker AXS, Karlsruhe, Germany). Instrument contributions were taken into account by using a measured instrument function for reflection profiles. Peak shapes were modeled using modified Thompson–Cox–Hastings pseudo-Voigt profiles [22, 23]. The background was fitted with Chebychev polynomials up to the 12th order. The lattice parameters derived from the Rietveld refinement agree well with those obtained from the single-crystal data (see Table 1). Figure 1 shows the result of the Rietveld refinement of $Li_2Pt_3Se_4$. Elemental platinum [26], $PtSe_2$ [27], and Pt_5Se_4 [28] were always present in different amounts as by-products. The bulk samples of $Ag_2Pd_3Se_4$ and $Cu_2Pd_3Se_4$ from high-pressure experiments indicated a low degree of crystallinity, and powder refinements resulted in no precise lattice parameters. Nevertheless, some single crystals suitable for X-ray diffraction were identified inside the bulk samples.

By mechanical fragmentation, several irregularly shaped silvery crystals were isolated from the crushed samples treated under high-pressure/high-temperature conditions. For better handling, the crystal fragments were embedded in perfluoropolyalkylether (viscosity 1800 cSt) and fixed on thin glass fibers with high-vacuum grease. The intensity data collections of the $Cu_2Pd_3Se_4$ and $Li_2Pt_3Se_4$ crystals were carried out on a Nonius Kappa-CCD diffractometer with graphite-monochromatized MoK_α radiation (λ = 71.07 pm) at room temperature. The program SCALEPACK [24] was used to correct the intensity data for absorption based on equivalent and redundant intensities. For the $Ag_2Pd_3Se_4$ single-crystal data collection, a Bruker D8 Quest diffractometer with a Photon 100 detector system and an Incoatec Microfocus source generator (multi layered optics-monochromatized MoK_α radiation, λ = 71.07 pm) was used. Collection strategies, concerning ω and φ scans, were optimized with the APEX-2 program package [25], resulting in data sets of complete reciprocal spheres up to high angles with high completeness. Reflection intensities were integrated with the program SAINT [25] using a narrow-frame algorithm and corrected for absorption effects with the program SADABS [25], based on the semi-empirical multi-scan approach. Table 1 summarizes the experimental details.

3 Results and discussion

3.1 Structure refinements

For all three compounds the systematic extinctions $h0l$ with $l \neq 2n$, $0k0$ with $k \neq 2n$, and $00l$ with $l \neq 2n$ were

Table 1: Crystal data and structure refinements of $Li_2Pt_3Se_4$ and the isostructural compounds $Ag_2Pd_3Se_4$ and $Cu_2Pd_3Se_4$.

	$Li_2Pt_3Se_4$	$Ag_2Pd_3Se_4$	$Cu_2Pd_3Se_4$
Molar mass, g·mol^{-1}	914.99	850.78	762.12
Crystal system	Monoclinic	Monoclinic	Monoclinic
Space group	$P2_1/c$ (no. 14)	$P2_1/c$ (no. 14)	$P2_1/c$ (no. 14)
Cell formula units	2	2	2
Powder diffractometer	STOE Stadi P		
Radiation	Mo$K_{\alpha1}$ (λ = 70.93 pm)		
Powder data			
a, pm	525.60(2)		
b, pm	1039.94(3)		
c, pm	636.12(2)		
β, deg	111.92(3)		
V, Å^3	322.55(2)		
Single-crystal diffractometer	Nonius Kappa CCD	Bruker D8 Quest	Nonius Kappa CCD
Radiation	MoK_α (λ = 71.073 pm)	MoK_α (λ = 71.073 pm)	MoK_α (λ = 71.073 pm)
Single-crystal data:			
a, pm	525.9(2)	563.46(3)	563.8(2)
b, pm	1040.6(2)	1039.89(6)	986.6(2)
c, pm	636.5(2)	637.72(4)	624.3(2)
β, deg	111.91(3)	115.103(2)	115.40(3)
V, Å^3	323.1(2)	338.37(3)	313.7(2)
Calculated density, g·cm^{-3}	9.40	8.35	8.07
Crystal size, mm^3	0.04 × 0.02 × 0.01	0.015 × 0.024 × 0.063	0.04 × 0.03 × 0.03
Absorption coefficient, mm^{-1}	87.2	34.9	38.2
F(000), e	752	736	664
Detector distance, mm	36	40	36
θ range, deg	3.9–32.47	3.92–32.43	4.00–32.50
Range in *hkl*	±7, ±5, ±9	±8, ±15, ±9	±8, ±14, ±9
Total no. reflections	4481	12 566	4330
Data/ref. parameters	1168/44	1221/54	1142/54
Reflections with $I > 2\sigma(I)$	1118	1161	1104
R_{int}/R_σ	0.0602/0.0386	0.0332/0.0159	0.0435/0.0314
Absorption correction	Multi-scan [24]	Multi-scan [25]	Multi-scan [24]
Goodness-of-Fit on F^2	1.156	1.120	1.296
*R*1/*wR*2 for $I > 2\sigma(I)$	0.0246/0.0562	0.0325/0.0712	0.0460/0.1000
*R*1/*wR*2 for all data	0.0269/0.0569	0.0350/0.0721	0.0482/0.0994
Extinction coefficient	0.0022(2)	0.0037(3)	0.0037(5)
Largest diff. peak/hole, e·Å^{-3}	3.77/−2.10	3.53/−2.14	2.51/−2.17

Standard deviations are given in parentheses.

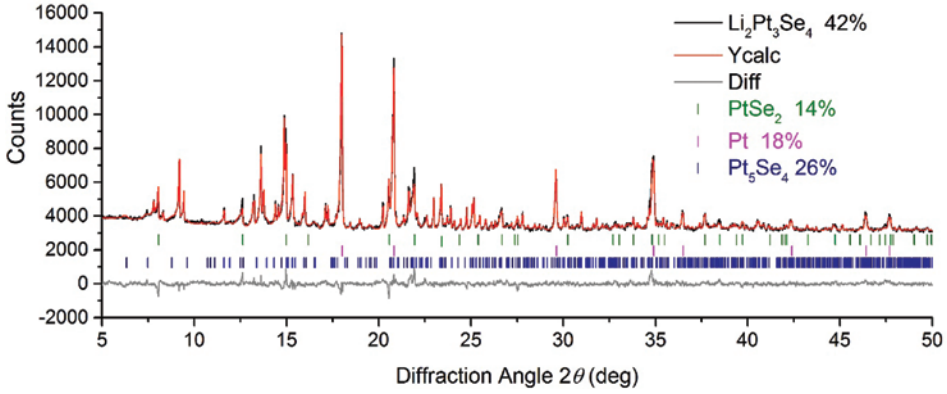

Fig. 1: XRD pattern (Mo$K_{\alpha1}$ radiation) of $Li_2Pt_3Se_4$, simultaneously refined with Pt [26], $PtSe_2$ [27], and Pt_5Se_4 [28] (R_{exp} = 1.65, R_{wp} = 2.57, R_p = 1.85, and GOF = 1.56).

evident and led to the space group $P2_1/c$ (no. 14). The initial positional parameters were deduced from an automatic interpretation of Direct Methods with SHELXS-2013 [29], and the following full-matrix least-squares refinements on F^2 were performed with SHELXL-2013 [30, 31]. In the case of $Li_2Pt_3Se_4$, the positional parameters of the isostructural compound $Li_2Pt_3S_4$ [7] were used as starting values for the structure refinement. To

Table 2: Atomic coordinates and isotropic equivalent displacement parameters U_{eq} (Å^2) for $Li_2Pt_3Se_4$, $Ag_2Pd_3Se_4$, and $Cu_2Pd_3Se_4$ (space group: $P2_1/c$, $Z = 2$).

Atom	Wyckoff-Position	sof	x	y	z	U_{eq}
$Li_2Pt_3Se_4$						
Pt1	4*e*	1	0.26919(5)	0.37126(2)	0.02280(4)	0.00643(9)
Pt2	2*a*	1	0	0	0	0.00642(9)
Se1	4*e*	1	0.0310(2)	0.31004(6)	0.2767(1)	0.0066(2)
Se2	4*e*	1	0.4728(2)	0.05395(6)	0.2560(2)	0.0070(2)
Li	4*e*	1	0.615(3)	0.301(2)	0.461(2)	0.020(3)
$Ag_2Pd_3Se_4$						
Pd1a	4*e*	0.916(6)	0.2615(2)	0.12506(7)	0.5063(2)	0.0103(2)
Pd1b	4*e*	0.084(6)	0.167(3)	0.103(1)	0.471(2)	0.017(2)
Ag1a	4*e*	0.902(5)	0.6299(2)	0.19673(8)	0.9827(2)	0.0183(2)
Ag1b	4*e*	0.098(5)	0.547(2)	0.2248(8)	0.992(2)	0.018(2)
Pd2	2*a*	1	0	0	0	0.0111(2)
Se1	4*e*	1	0.0467(2)	0.31729(6)	0.2637(2)	0.0127(2)
Se2	4*e*	1	0.4665(2)	0.05206(6)	0.2549(2)	0.0126(2)
$Cu_2Pd_3Se_4$						
Pd1a	4*e*	0.953(6)	0.2561(2)	0.12684(9)	0.4986(2)	0.0112(3)
Pd1b	4*e*	0.047(3)	0.154(6)	0.089(3)	0.472(4)	0.028(6)
Cu1a	4*e*	0.95(2)	0.6148(8)	0.1928(4)	0.9799(3)	0.0225(7)
Cu1b	4*e*	0.05(2)	0.54(1)	0.227(5)	0.972(4)	0.012(8)
Pd2	2*a*	1	0	0	0	0.0115(2)
Se1	4*e*	1	0.0134(2)	0.3137(2)	0.2359(2)	0.0123(2)
Se2	4*e*	1	0.4706(2)	0.0552(2)	0.2420(2)	0.0126(2)

U_{eq} is defined as one third of the trace of the orthogonalized U_{ij} tensor. Standard deviations are given in parentheses.

Table 3: Anisotropic displacement parameters (Å^2) for $Li_2Pt_3Se_4$, $Ag_2Pd_3Se_4$, and $Cu_2Pd_3Se_4$ (space group: $P2_1/c$, $Z = 2$).

Atom	U_{11}	U_{22}	U_{33}	U_{23}	U_{13}	U_{12}
$Li_2Pt_3Se_4$						
Pt1	0.0073(2)	0.0060(2)	0.0071(2)	– 0.00011(7)	0.00390(9)	– 0.00081(7)
Pt2	0.0067(2)	0.0059(2)	0.0075(2)	0.0004(2)	0.0037(2)	– 0.00023(9)
Se1	0.0075(3)	0.0060(2)	0.0074(3)	– 0.0003(2)	0.0042(2)	0.0003(2)
Se2	0.0074(3)	0.0066(2)	0.0079(3)	0.0005(2)	0.0040(2)	0.0005(2)
Li	0.017(6)	0.030(7)	0.014(6)	0.004(5)	0.005(5)	0.013(5)
$Ag_2Pd_3Se_4$						
Pd1a	0.0144(5)	0.0100(3)	0.0079(3)	0.0012(2)	0.0060(3)	0.0028(3)
Ag1a	0.0169(4)	0.0149(3)	0.0223(3)	– 0.0031(2)	0.0079(2)	– 0.0029(3)
Pd2	0.0162(3)	0.0085(3)	0.0100(3)	– 0.0004(2)	0.0073(2)	– 0.0022(2)
Se1	0.0203(3)	0.0096(3)	0.0114(3)	0.0013(2)	0.0100(2)	0.0032(2)
Se2	0.0176(3)	0.0120(3)	0.0098(2)	0.0020(2)	0.0072(2)	0.0026(2)
$Cu_2Pd_3Se_4$						
Pd1a	0.0132(4)	0.0137(4)	0.0076(3)	0.0010(2)	0.0054(3)	0.0027(3)
Cu1a	0.019(2)	0.022(2)	0.0271(8)	– 0.0035(6)	0.0112(6)	– 0.004(2)
Pd2	0.0125(4)	0.0143(4)	0.0081(4)	0.0007(3)	0.0049(3)	– 0.0013(3)
Se1	0.0144(4)	0.0147(4)	0.0090(4)	0.0001(3)	0.0060(3)	0.0012(3)
Se2	0.0134(4)	0.0164(4)	0.0088(4)	0.0017(3)	0.0055(3)	0.0019(3)

Standard deviations are given in parentheses.

verify the correct compositions of $Li_2Pt_3Se_4$, $Cu_2Pd_3Se_4$, and $Ag_2Pd_3Se_4$, all occupancy parameters were refined in separate series of least-squares cycles. All sites were fully occupied within two standard deviations. Furthermore, all sites were refined with anisotropic displacement parameters, but only for $Li_2Pt_3Se_4$ the final Fourier synthesis did not reveal any significant residual peaks (see Table 1). The positional parameters as starting values for the refinement of $Ag_2Pd_3Se_4$ were derived from $Cu_2Pd_3Se_3$ with the Cu^+ position taken for Ag^+. A refinement of a possible mixed occupation of Pd sites with Cu or Ag resulted in higher *R* values even if, in the case of $Ag_2Pd_3Se_4$, there are only slight differences in the scattering factors of Ag^+ and Pd^{2+}. Moreover, geometrical aspects, which will be discussed later, are in favor of a clear distinction between Pd^{2+} sites on the one hand and Cu^+ or Ag^+ sites on the other.

The refinements of the synthetic mineral phases $Cu_2Pd_3Se_4$ and $Ag_2Pd_3Se_4$ exhibited considerable residual peaks in distances of 0.65(5) Å from the Cu1, Ag1, and Pd1 sites. As a consequence, a split-atom model of the Cu1 and Pd1 sites in $Cu_2Pd_3Se_4$ as well as of the Ag1 and Pd1 sites in $Ag_2Pd_3Se_4$, was evident in separate difference-Fourier syntheses. The additional split sites were refined with isotropic displacement parameters. Due to high correlation factors, refinements with anisotropic displacement parameters were not reasonable. The splitting of the sites in $Ag_2Pd_3Se_4$ was about twice as pronounced as in

Table 4: Interatomic distances (pm) of $Li_2Pt_3Se_4$, $Ag_2Pd_3Se_4$, and $Cu_2Pd_3Se_4$.

$Li_2Pt_3Se_4$				$Ag_2Pd_3Se_4$				$Cu_2Pd_3Se_4$			
Pt1:	Se2	244.8(1)		Pd1a:	Pd1b	53.5(1)		Pd1a:	Pd1b	64.4(1)	
	Se2	245.2(1)			Se2	246.0(1)			Se1	245.7(2)	
	Se1	246.9(1)			Se2	246.6(1)			Se2	246.6(2)	
	Se1	247.3(1)			Se1	249.1(1)			Se1	248.0(2)	
	Li	268.8(17)			Se1	250.3(1)			Se2	248.8(2)	
	Li	279.8(13)			Ag1b	227.1(1)			Cu1b	222.5(1)	
Pt2:	Se1	247.5(1)	2×		Ag1a	283.4(2)			Cu1a	273.4(5)	
	Se2	247.6(1)	2×		Ag1a	295.7(2)			Cu1b	286.9(1)	
	Li	283.9(17)	2×		Ag1b	300.5(1)			Cu1a	288.6(2)	
Li:	Se1	262.3(13)		Ag1a:	Ag1b	57.6(1)		Cu1a:	Cu1b	51.4(1)	
	Pt1	268.8(17)			Se1	259.4(1)			Se1	243.8(2)	
	Se2	272.2(14)			Se2	273.5(1)			Se2	251.4(2)	
	Pt2	283.9(17)			Se2	293.0(2)			Se2	275.1(4)	
	Se1	284.2(15)			Se2	294.1(2)			Se2	283.0(4)	
	Se2	292.5(15)			Se1	297.9(2)			Se1	306.4(2)	
	Li	335.6(10)	2×		Se1	320.5(2)			Se1	321.1(1)	
					Pd1b	331.4(1)			Pd1b	328.4(2)	
					Pd1b	334.5(1)			Pd1b	335.7(1)	
				Pd1b:	Se1	238.9(8)		Pd1b:	Se1	232(2)	
					Se1	253.2(8)			Se2	254(2)	
					Se2	261.9(10)			Se1	259(2)	
					Se2	264.6(10)			Se2	275(3)	
					Ag1b	275.1(9)			Cu1b	285(8)	
					Ag1b	334.7(9)			Cu1b	324(6)	
				Ag1b:	Se1	260.2(9)		Cu1b:	Se2	252(4)	
					Se2	262.4(6)			Se2	255(3)	
					Se2	270.1(7)			Se1	259(4)	
					Se1	277.9(8)			Se1	273(4)	
					Se2	326.7(7)			Se2	307(6)	
					Se1	370.5(8)			Se1	356(6)	
				Pd2:	Se2	249.4(1)	2×	Pd2:	Se2	248.6(2)	2×
					Se1	250.7(1)	2×		Se1	249.2(1)	2×
					Ag1a	289.0(1)	2×		Cu1a	284.9(5)	2×
					Pd1b	294.1(1)			Pd1b	283(2)	
					Pd1a	320.2(1)			Pd1a	308.0(2)	
					Ag1b	344.6(1)			Cu1b	336.2(1)	

Standard deviations are given in parentheses.

$Cu_2Pd_3Se_4$. About 10% of the Ag1 and Pd1 atoms of $Ag_2Pd_3Se_4$ occupy additional split sites, whereas in $Cu_2Pd_3Se_4$ about 5% of Cu1 and Pd1 are distributed over two positions. Without refinement of the split positions, the *R* values of $Ag_2Pd_3Se_4$ and $Cu_2Pd_3Se_4$ are *R1* = 0.0685/*wR2* = 0.1704 and *R1* = 0.0654/*wR2* = 0.1441, respectively. A refinement including the split positions resulted in considerably better *R* values of *R1* = 0.0325/*wR2* = 0.0721 for $Ag_2Pd_3Se_4$ and *R1* = 0.0460/*wR2* = 0.1000 for $Cu_2Pd_3Se_4$. Final Fourier syntheses revealed negligible residual peaks in distances of 0.70(2) Å next to Se1 and Se2. A refinement of other split positions was neglected. Non-merohedral twinning as a possible reason for the structural disorder was checked carefully but no evidence could be found. Small epitaxially grown crystals, which could be indexed with CELL_NOW [25], are in our opinion not the reason for the observed structural disorder as their scattering intensity contributed only about 1% to the total scattering of the main component. Details of the single-crystal structure measurements are shown in Table 1, and the positional parameters (Table 2), anisotropic displacement parameters (Table 3), interatomic distances, and angles (Tables 4 and 5) are listed additionally.

Further details of the crystal structure investigations may be obtained from Fachinformationszentrum Karlsruhe, 76344 Eggenstein-Leopoldshafen, Germany (fax: +49-7247-808-666; e-mail: crysdata@fiz-karlsruhe.de, http://www.fiz-karlsruhe.de/request_for_deposited_data.html) on quoting the deposition numbers CSD-431596 ($Li_2Pt_3Se_4$), CSD-431597 ($Ag_2Pd_3Se_4$), and CSD-431598 ($Cu_2Pd_3Se_4$).

3.2 Crystal chemistry

As already mentioned, the lithium platinum selenide, $Li_2Pt_3Se_4$ presented here, which was synthesized under high-pressure/high-temperature conditions of 8 GPa and 1200°C, crystallizes isostructurally to the corresponding sulfides $Li_2M_3S_4$ (*M* = Pd, Pt) [7], and to the minerals chrisstanleyite ($Ag_2Pd_3Se_4$) and jaguéite ($Cu_2Pd_3Se_4$) [3]. Synthesis attempts for the missing compound $Li_2Pd_3Se_4$ have failed so far, resulting in binary lithium selenide and various palladium selenides. Normal-pressure experiments in sealed silica ampoules were also performed without success. According to Vymazalová [4], the mineral chrisstanleyite is only stable at temperatures below 430°C. Our experiments to synthesize $Li_2M_3X_4$ (*M* = Pd, Pt, *X* = S, Se) compounds exceeded this temperature significantly. Repetitions of the experiments at low temperatures are still pending. In Table 6 the lattice parameters of the known isostructural compounds are summarized.

The crystal structure of $Li_2Pt_3Se_4$ is built up from two distinct Pt sites (Pt1 on a general position; Pt2 on the special position at 0, 0, 0), two general selenium sites, and one general lithium site (see Table 2). Both Pt atoms are in a nearly square planar Se coordination with Pt–Se distances ranging from 244.8 to 247.5 pm. There are distinct differences between the two Pt sites, however. The atoms Pt2 occur in single $PtSe_4$ units, whereas the atoms Pt1 form pairs of square planar $PtSe_4$ units paired *via* a common Se2–Se2 edge and resulting in Pt1–Pt1 distances of 406.1(1) pm (see Fig. 2). These two units (single and paired $PtSe_4$ units) build up a three-dimensional open network structure by linking the units through common corners. As a result of the arrangement of the $PtSe_4$ units, channels

Table 5: Selected interatomic angles (deg) of $Li_2Pt_3Se_4$, $Ag_2Pd_3Se_4$, and $Cu_2Pd_3Se_4$.

$Li_2Pt_3Se_4$		
Se2–Pt1–Se2	81.97(3)	
Se1–Pt1–Se1	87.53(2)	
Se2–Pt1–Se1	93.00(3)	
Se2–Pt1–Se1	97.55(2)	
Se2–Pt1–Se1	174.88(2)	
Se2–Pt1–Se1	174.90(2)	
Se1–Pt2–Se2	86.08(3)	2×
Se1–Pt2–Se2	93.92(3)	2×
Se1–Pt2–Se1	180.0	
Se2–Pt2–Se2	180.0	
$Ag_2Pd_3Se_4$		
Se2–Pd1a–Se2	80.19(6)	
Se1–Pd1a–Se1	88.53(7)	
Se2–Pd1a–Se1	94.89(8)	
Se2–Pd1a–Se1	96.74(8)	
Se2–Pd1a–Se1	172.1(1)	
Se2–Pd1a–Se1	175.3(2)	
Se2–Pd2–Se1	82.93(2)	2×
Se2–Pd2–Se1	97.07(2)	2×
Se1–Pd2–Se1	180.0	
Se2–Pd2–Se2	180.0	
$Cu_2Pd_3Se_4$		
Se2–Pd1a–Se2	82.95(6)	
Se1–Pd1a–Se1	85.90(5)	
Se1–Pd1a–Se2	94.01(7)	
Se2–Pd1a–Se1	97.36(7)	
Se1–Pd1a–Se2	175.4(2)	
Se1–Pd1a–Se2	175.8(2)	
Se2–Pd2–Se1	85.02(4)	2×
Se2–Pd2–Se1	94.98(4)	2×
Se1–Pd2–Se1	180.0	
Se2–Pd2–Se2	180.0	

Standard deviations are given in parentheses.

Table 6: Comparison of lattice parameters (pm) of the isostructural compounds $Li_2Pt_3S_4$, $Li_2Pd_3S_4$, and the minerals chrisstanleyite and jaguéite.

Compound	*a*	*b*	*c*	*β*
$Li_2Pt_3Se_4$ (this work)	525.9(2)	1040.6(2)	636.5(2)	111.91(3)°
$Li_2Pt_3S_4$ [7]	498.2(1)	1005.5(2)	613.0(2)	110.76(3)°
$Li_2Pd_3S_4$ [7]	492.9(1)	1005.9(2)	614.9(2)	110.91(3)°
$Ag_2Pd_3Se_4$ (this work)	563.46(3)	1039.89(6)	637.72(4)	115.103(2)°
Chrisstanleyite [3]	567.6(2)	1034.2(4)	634.1(2)	114.996(4)°
$Cu_2Pd_3Se_4$ (this work)	563.8(2)	986.6(2)	624.3(2)	115.40(3)°
Jaguéite [3]	567.2(5)	990.9(9)	626.4(6)	115.40(2)°

Standard deviations are given in parentheses.

are created, in which the lithium atoms are located. Figure 2 shows the crystal structure of $Li_2Pt_3Se_4$ viewed along the crystallographic *a* and *c* axes, respectively. For a more detailed description of the crystal structure, the reader is referred to the references [3, 7]. A comparison of $Li_2Pt_3Se_4$ and the synthetic mineral phases chrisstanleyite ($Ag_2Pd_3Se_4$) and jaguéite ($Cu_2Pd_3Se_4$) is given below.

As already mentioned in the introduction, Paar [1, 2] described chrisstanleyite and jaguéite as commonly occurring, partially intergrown minerals, with a mixed (Ag, Cu) occupancy. Twenty percent of the silver atoms in chrisstanleyite are substituted by copper and 5% of the copper atoms in jaguéite are replaced by silver resulting in the corresponding compounds $Ag_{1.6}Cu_{0.4}Pd_3Se_4$ (chrisstanleyite) and $Cu_{1.9}Ag_{0.1}Pd_3Se_4$ (jaguéite). In the case of chrisstanleyite, Topa refined the mixed occupancy with equal isotropic displacement factors, but with free positional parameters [3] creating additional sites. For natural jaguéite no mixed occupancies were refined by Topa. The appearance of additional sites in this structure type is rather a stabilizing effect of an optimized network of metal-metal bonds than an effect of differences in the ionic radii of silver (Ag^+ C.N. 6: 1.29 Å [32]) and copper (Cu^+ C.N. 6: 0.91 Å [32]). This can be concluded from the refinements of the pure synthetic minerals presented here which show a comparable splitting of the copper and silver sites, without an occupation of the split sites with different atom types. Furthermore, for the Pd1 sites of the synthetic minerals a refinement of hitherto not described split positions at distances of 0.53 Å ($Ag_2Pd_3Se_4$) and 0.64 Å ($Cu_2Pd_3Se_4$) resulted in significantly better *R* values. Overall, the effect of layer splitting is more pronounced in $Ag_2Pd_3Se_4$ (Ag1a/Ag1b: 0.90(1)/0.10(1); Pd1a/Pd1b: 0.92(1)/0.08(1)) than in $Cu_2Pd_3Se_4$ (Cu1a/Cu1b: 0.94(2)/0.06(2); Pd1a/Pd1b: 0.95(1)/0.05(1)). Most likely, copper and silver occur strictly in the oxidation state +1 in these compounds. The occurrence of Cu^{2+} (or Ag^{2+}) ions in a mixed occupation of the Pd1a/Pd1b sites as reason for the structural disorder is rather unlikely, but cannot be completely excluded. As already mentioned above, the *R* values worsen when the disorder is taken into accont. Moreover, the d^8 Pd^{2+} ions gain a significantly better stabilization in the square planar ligand field than d^9-configured Cu^{2+} (or Ag^{2+}) ions would get. Magnetic measurements to confirm the exclusive +1 oxidation state of copper and silver have not been attempted as yet. Unfortunately, up to now we were not able to optimize the synthesis of $Cu_2Pd_3Se_4$ in such a way as to obtain pure products without

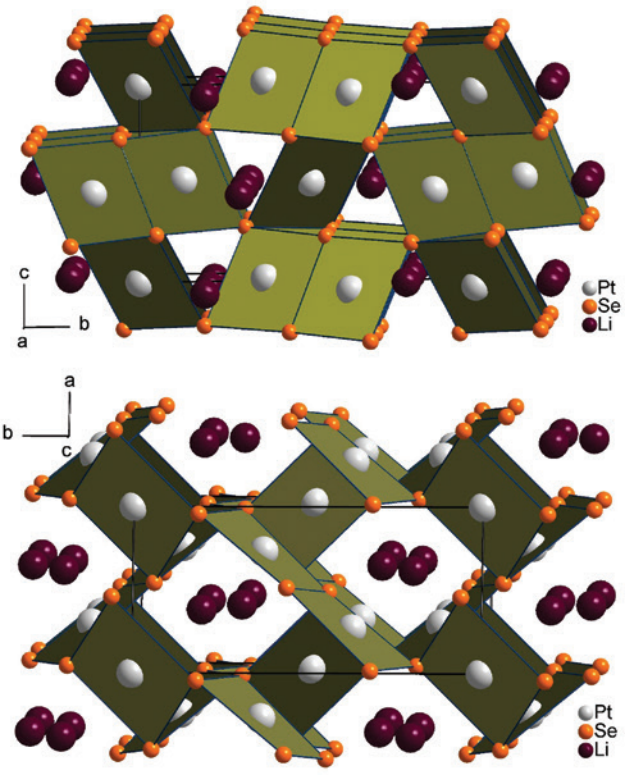

Fig. 2: Crystal structures of $Li_2Pt_3Se_4$ as viewed along the crystallographic *a* (top) and *c* axes (down). Lithium, platinum and selenium are drawn as dark purple, light gray and orange circles, respectively. Relevant $PtSe_4$ polyhedra are emphasized.

side phases, which is a premise for meaningful magnetic measurements.

The replacement of Cu^+/Ag^+ by lithium (Li^+ C.N.6: 0.90 Å [32]) in $Li_2Pt_3Se_4$ and the isostructural compounds $Li_2Pt_3S_4$ and $Li_2Pd_3S_4$ [7] leads to the absence of split positions. Figure 3 shows the stabilizing metal–metal bond system of this structure type mentioned above, consisting of a nearly collinear sequence of four metal–metal bonds with distances of 268.8–283.9 pm ($Li_2Pt_3Se_4$). The Pt1–Li1–Pt2–Li1–Pt1 sequences are interconnected *via* Pt1–Li1 bonds to zig-zag layers parallel to the *bc* plane. A comparable situation can be found for the isostructural compounds $Li_2Pd_3S_4$ and $Li_2Pt_3S_4$ with Li–Pd and Li–Pt contacts varying from 260.5–283.1 pm and 259.7–285.0 pm, respectively [7]. In Fig. 4, a cutout of the collinear metal–metal sequence demonstrates the different bonding situations in $Li_2Pt_3Se_4$ and $Ag_2Pd_3Se_4$. All contacts shorter than 301 pm are drawn as bonds. The metal–metal distances in $Li_2Pt_3Se_4$ are less different and the contacts interconnecting the collinear sequences are much shorter than in $Ag_2Pd_3Se_4$. With implementation of the additional split sites (split atoms are labeled with appendix a and b in Fig. 4) in $Ag_2Pd_3Se_4$, two shorter Ag1b–Pd1a and Ag1b–Pd1b contacts of 227 pm and 275 pm become prominent, whereas the Ag1b–Pd2 contact is elongated up to 344 pm. Therefore, the Pd2 atoms remain isolated and the collinear metal-metal sequence changes into an alternating Ag1–Pd1 zig-zag sequence in the direction along the *c* axis. For $Cu_2Pd_3Se_4$ (not shown) the situation is comparable.

Differences between the lithium-containing compounds and the mineral phases regarding the coordination of lithium, silver and copper are evident. Topa [3] described the coordination polyhedra of copper and silver as strongly elongated tetrahedra with Cu–Se distances of 244.4–285.7 pm for jaguéite, and Ag–Se distances of 259.0–294.8 pm for chrisstanleyite. The lithium atoms in $Li_2M_3X_4$ (M = Pd, Pt, X = S, Se) are coordinated by six chalcogenide atoms in a distorted trigonal prismatic coordination geometry. The distances range from 249.8–288.5 pm for $Li_2Pd_3S_4$, 247.9–288.6 pm for $Li_2Pt_3S_4$, and 262.3–292.5 pm for $Li_2Pt_3Se_4$ (see Table 4). In Fig. 5 the lithium, silver and copper coordination polyhedra are shown with relevant distances. $Li_2Pt_3Se_4$ exhibits

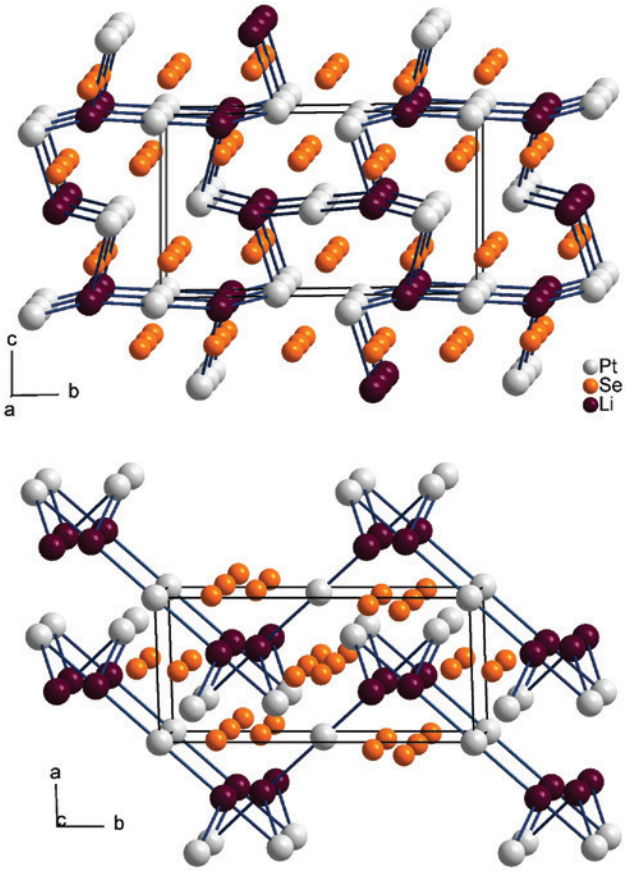

Fig. 3: Crystal structure of $Li_2Pt_3Se_4$ as viewed along the *a* (top) and *c* axes (down) with Li–Pt metal–metal bonds drawn in a collinear sequence Pd2–Li–Pd1–Li–Pd2. Lithium, platinum and selenium are drawn as dark purple, light gray and orange circles, respectively.

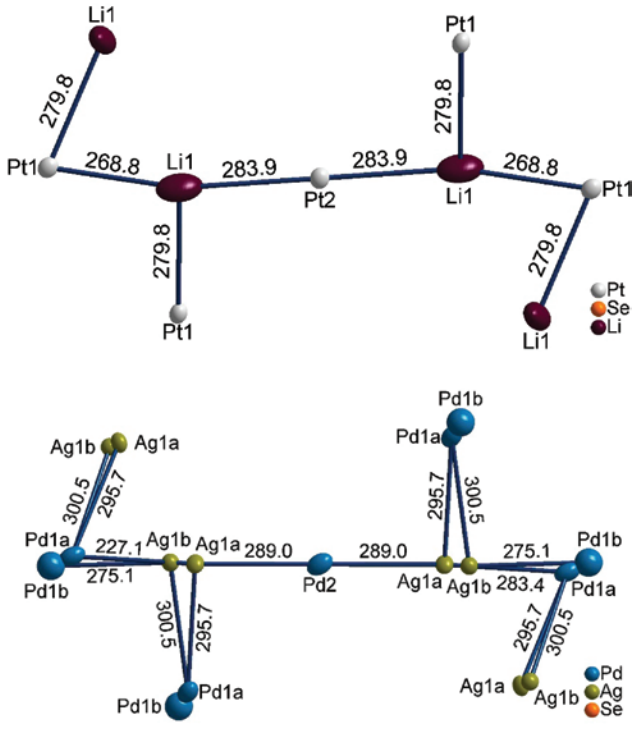

Fig. 4: Collinear sequence of Pt1-Li1-Pt2-Li1-Pt1 in $Li_2Pt_3Se_4$ (top) and corresponding sequence in $Ag_2Pd_3Se_4$ (down) with Pd1 and Ag1 split positions. Atom distances shorter than 301 pm are drawn as bonds. All distances are given in pm.

two short Li–Se contacts (262.3 pm, 272.2 pm) and four longer (284.2–292.5 pm) ones (see Table 4). Nevertheless, the distances are more uniform than in $Ag_2Pd_3Se_4$ and $Cu_2Pd_3Se_4$. Between the shortest and the longest contacts in $Li_2Pt_3Se_4$, a difference of 30 pm occurs. Considering the same distance criterion for the compounds $Ag_2Pd_3Se_4$ and $Cu_2Pd_3Se_4$, only two Se atoms appear inside the coordination sphere. For a tetrahedral coordination of Ag1a and Cu1a, the minimum spread of the four Ag–Se and Cu–Se distances are 35 pm and 39 pm, respectively. Significantly more pronounced is the difference between the shortest and longest contacts, assuming a trigonal prismatic coordination of Ag (61 pm) and Cu (77 pm) as shown for $Li_2M_3X_4$ (M = Pd, Pt, X = S, Se). As a result of the split positions, the effect increases even more, and the coordination of Ag and Cu moves towards a square planar coordination sphere.

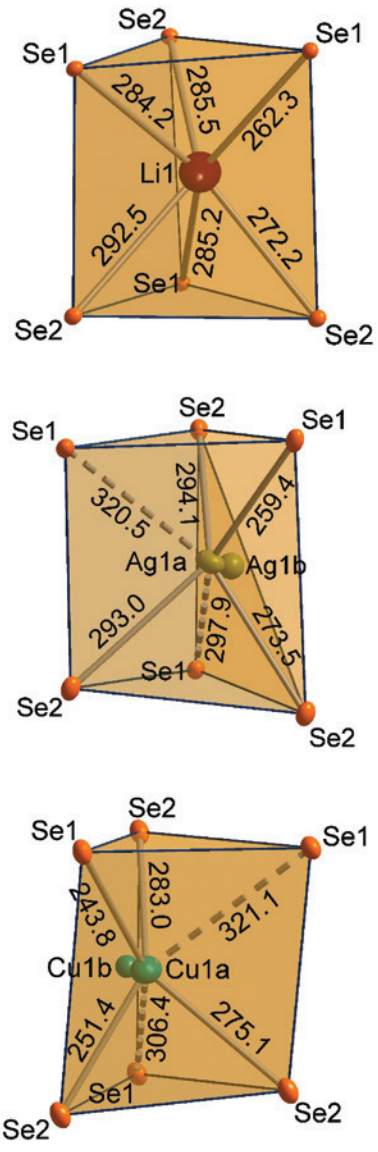

Fig. 5: The distorted trigonal prismatic selenium coordination polyhedra of the Li, Ag, and Cu atoms in $Li_2Pt_3Se_4$ (top), $Ag_2Pd_3Se_4$ (middle), and $Cu_2Pd_3Se_4$ (down) are shown, respectively. All distances are given in pm.

4 Conclusion

$Li_2Pt_3Se_4$, showing a structure analogous to $Li_2M_3S_4$ (M = Pd, Pt), was synthesized under high-pressure/high-temperature conditions of 8 GPa and 1200°C. Under the same conditions the isostructural minerals jaguéite ($Cu_2Pd_3Se_4$) and chrisstanleyite ($Ag_2Pd_3Se_4$) were reproduced in their ideal stoichiometric ratio and investigated by single-crystal X-ray analysis. In contrast to the structure refinements of Topa [3], a disorder phenomenon was observed for the synthetic mineral phases. Structural differences, especially with regard to the coordination environments, were identified and analyzed in this work.

Acknowledgments: We would like to thank Prof. Dr. H. Huppertz for continuous support and access to all the facilities of the Institute of General, Inorganic and Theoretical Chemistry, University of Innsbruck. For discussion and support regarding the single-crystal refinements we thank Dr. Klaus Wurst, University of Innsbruck. Dr. G. Heymann is supported by the program Nachwuchsförderung of the University of Innsbruck.

References

[1] W. H. Paar, D. Topa, E. Makovicky, R. J. Sureda, M. K. de Brodtkorb, E. H. Nickel, H. Putz, *Can. Mineral.* **2004**, *42*, 1745.
[2] W. H. Paar, A. C. Roberts, A. J. Criddle, D. Topa, *Mineral. Mag.* **1998**, *62*, 257.
[3] D. Topa, E. Makovicky, T. Balić-Žunić, *Can. Mineral.* **2006**, *44*, 497.
[4] A. Vymazalová, D. A. Chareev, A. V. Kristavchuk, F. Laufek, M. Drábek, *Can. Mineral.* **2014**, *52*, 77.
[5] F. Laufek, A. Vymazalová, D. A. Chareev, A. V. Kristavchuk, Q. Lin, J. Drahokoupil, T. M. Vasilchikova, *J. Solid State Chem.* **2011**, *184*, 2794.
[6] F. Laufek, A. Vymazalová, D. A. Chareev, A. V. Kristavchuk, J. Drahokoupil, M. V. Voronin, *Powder Diffr.* **2013**, *28*, 13.
[7] G. Heymann, O. Niehaus, H. Krüger, P. Selter, G. Brunklaus, R. Pöttgen, *J. Solid State Chem.* **2016**, *242*, 87.
[8] R. Ang, Y. Miyata, E. Ieki, K. Nakayama, T. Sato, Y. Liu, W. J. Lu, Y. P. Sun, T. Takahashi, *Phys. Rev. B: Condens. Matter* **2013**, *88*, 115145.
[9] S. Nagata, T. Atake, *J. Therm. Anal. Calorim.* **1999**, *57*, 807.
[10] A. P. Ramirez, R. J. Cava, J. Krajewski, *Nature* **1997**, *386*, 156.

[11] O. Lang, C. Felser, R. Seshadri, F. Renz, J. M. Kiat, J. Ensling, P. Gütlich, W. Tremel, *Adv. Mater.* **2000**, *12*, 65.
[12] R. Pocha, C. Löhnert, D. Johrendt, *J. Solid State Chem.* **2007**, *180*, 191.
[13] W. Tremel, H. Kleinke, V. Derstroff, C. Reisner, *J. Alloys Compd.* **1995**, *219*, 73.
[14] T. Hughbanks, *J. Alloys Compd.* **1995**, *229*, 40.
[15] J. Cabana, L. Monconduit, D. Larcher, M. R. Palacín, *Adv. Mater.* **2010**, *22*, E170.
[16] D. Chen, G. Ji, B. Ding, Y. Ma, B. Qu, W. Chen, J. Y. Lee, *Ind. Eng. Chem. Res.* **2014**, *53*, 17901.
[17] X. Xu, W. Liu, Y. Kim, J. Cho, *Nano Today* **2014**, *9*, 604.
[18] H. Huppertz, *Z. Kristallogr.* **2004**, *219*, 330.
[19] D. Walker, M. A. Carpenter, C. M. Hitch, *Am. Mineral.* **1990**, *75*, 1020.
[20] D. Walker, *Am. Mineral.* **1991**, *76*, 1092.
[21] D. C. Rubie, *Phase Transit.* **1999**, *68*, 431.
[22] P. Thompson, D. E. Cox, J. B. Hastings, *J. Appl. Crystallogr.* **1987**, *20*, 79.
[23] R. A. Young, P. Desai, *Arch. Nauki. Mater.* **1989**, *10*, 71.
[24] Z. Otwinowski, W. Minor in *Methods in Enzymology,* Vol. 276, (Eds.: C. W. Charles, J. Carter and M. Sweet), Academic Press, USA, **1997**, p. 307.
[25] Apex2 (version 2014.11-0), Saint (version 8.34A), Sadabs (version 2014/5), and Cell_Now (version 2008/4), Bruker AXS GmbH, Karlsruhe (Germany).
[26] A. Gibaud, M. Topić, G. Corbel, C. I. Lang, *J. Alloys Compd.* **2009**, *484*, 168.
[27] F. Grønvold, H. Haraldsen, A. Kjekshus, *Acta Chem. Scand.* **1960**, *14*, 1879.
[28] P. Matković, K. Schubert, *J. Less-Common Met.* **1977**, *55*, 185.
[29] G. M. Sheldrick, Shelxs-2013, Program for the Solution of Crystal Structures, University of Göttingen, Göttingen (Germany) **2013**.
[30] G. M. Sheldrick, Shelxl-2013, Program for the Refinement of Crystal Structures – Multi-CPU Version, University of Göttingen, Göttingen (Germany) **2013**.
[31] G. Sheldrick, *Acta Crystallogr.* **2015**, *C71*, 3–8.
[32] N. Wiberg, *Lehrbuch der Anorganischen Chemie*, de Gruyter, Berlin, **2008**.